Vibrational Spectroscopic Properties of a $[C(NH_2)_3]_4Cl_2SO_4$ Ferroelectric Crystal — An Experimental and Theoretical Study

D. Podsiadła[a,*], O. Czupiński[b], D. Dudzic[c] and Z. Czapla[d,a]

[a]Institute of Experimental Physics, University of Wrocław, pl. M. Borna 9, 50-204 Wrocław, Poland

[b]Faculty of Chemistry, University of Wrocław, F. Joliot-Curie 14, 50-383 Wrocław, Poland

[c]Institute of Low Temperature and Structure Research of the Polish Academy of Sciences Okólna 2, 50-422 Wrocław, Poland

[d]Department of Physics, Opole University of Technology, Ozimska 75, 45-271 Opole, Poland

(Received August 30, 2013; in final form November 22, 2013)

Tetraguanidinium dichloride-sulphate crystal, $[C(NH_2)_3]_4Cl_2SO_4$, abbreviated as $G_4Cl_2SO_4$ was investigated. The vibrational infrared spectra of powdered $G_4Cl_2SO_4$ crystal in Nujol mull were studied in the wide range of temperature, from 298 K to 377 K. This temperature range contains all the phases in the crystal (named III, II, I on heating, respectively). The temperature changes of wavenumbers, centre of gravity, and intensity of the bands were analyzed to clarify the molecular mechanism of the phase transitions. It was shown that in cooling from 377 K to 313 K the phase II is the same as the room temperature phase. Information about hydrogen bonds was obtained. The time dependence of internal vibrations at 356 K was observed and it was connected with slow transition III → II. For more detailed band assignment Raman spectrum at room temperature, at ferroelectric phase was carried out. Theoretical calculations were made based on density functional theory, with the B3LYP method using 6-311 + G(d,p) basic set. Calculated normal vibrational modes of the molecule, their frequencies and intensities were compared with these recorded in experiment. Theoretical description of the molecule including hydrogen bonds were optimized and the bond parameters were obtained. The Mulliken charges population analysis was performed.

DOI: 10.12693/APhysPolA.125.115

PACS 78.30.−j, 78.20.Bh, 77.80.B−

1. Introduction

Crystals containing guanidinium cations and different inorganic salts or acids as anions have been extensively studied for years [1]. The guanidine is a small molecule and can be used as a component in supramolecular chemistry. Also the guanidinium cations — $[C(NH_2)_3]^+$ are found to exhibit interesting properties. The $[C(NH_2)_3]^+$ (signed as G) is a potential H-donor in hydrogen bonds because of its specific planar configuration. The detailed investigation of experimental and theoretical vibrational frequencies were carried out for the crystals containing guanidinium cations [2–5]. The reason is that the reliable assignment of the vibrational bands can be useful for understanding of the changes in hydrogen-bonded complexes.

Our current work also focuses on the studies of the experimental and theoretical vibrational modes of the new tetraguanidinium dichloride-sulphate crystal. The crystal, whose chemical formula is $[C(NH_2)_3]_4Cl_2SO_4$, abbreviated as $G_4Cl_2SO_4$ belongs to the family of crystals containing guanidinium cations.

Several various investigations for the crystal, as X-ray diffraction, calorimetric, dilatometric [6], dielectric and optical [6, 7] were performed. X-ray structural investigations [6] showed that the crystal is of orthorhombic symmetry of the space group $Cmc2_1$ (C_{2v}^{12}) at room temperature with four formula units per cell ($Z = 4$). The crystal is built of two anionic sublattices of monovalent Cl^- and divalent SO_4^{2-} anions and guanidinium cations [6]. There are three crystallographically different G ions in the structure, which are signed as G(1), G(2) and G(3). The prominent role of the stabilization of the crystal structure play hydrogen bonds. At room temperature X-ray diffraction data show seven N–H . . . Cl hydrogen bonds with an average distance of 3.390 Å and thirteen N–H . . . O hydrogen bonds with an average distance of 2.901 Å.

The sequential phase transitions (PTs) have been found in the crystal [6, 7]. The room temperature phase, which is a ferroelectric phase, is denoted as phase III. On ascending temperature $G_4Cl_2SO_4$ crystal shows two successive phase transitions of the first order at 353 K to the intermediate orthorhombic phase, denoted as phase II with the proposed space group $Fmm2$ (C_{2v}^{18}) ($Z = 4$) and at 357 K to the paraelectric tetragonal phase denoted as phase I with the space group $I\bar{4}2m$ (D_{2d}^{11}) ($Z = 2$), respectively (according to [6]). On descending temperature it shows only one PT, at 354 K, from the phase I to the phase II [7]. All the phase transitions are of the first order.

The sequence of the PTs in $[C(NH_2)_3]_4Cl_2SO_4$ is like follows:

III → PT 353 K → (III)II → PT 357 K → I (ascending temperature),

I → PT 354 K → II (descending temperature).

*corresponding author; e-mail: dorota@ifd.uni.wroc.pl

Coexistence of the phases III and II as well as the slow kinetics at the III → II phase transition was observed [6, 7].

The structures of the ferroelectric phase III and the paraelectric phase I are presented in [6]. In phase III the crystal is built of two anionic sublattices of monovalent Cl^-, divalent SO_4^{2-} anions and G cations, while in the phase I the structure is highly disordered. Despite the prominent order–disorder contribution to the transition mechanism the ferroelectric polarization in the crystal is of displacive-type [6].

Since the phase transitions in $G_4Cl_2SO_4$ crystal are due to the change in dynamical states of anions and cations, this should be related to the anomalies in shape and position of the absorption bands corresponding to the internal vibrations of the ions. So the infrared studies at different temperatures have been undertaken to study the molecular interactions contribution to the phase transition mechanisms. Time dependent measurements at constant temperature were taken in order to study the slow kinetics of phase transition III–II and the coexistence of these phases, as it was shown in [7].

The other purpose of this work is the comparison of the experimental vibrational spectra with the results of theoretical calculations. The proper assignment of bands in experimental spectrum is desired for a proper understanding of the spectral changes in the hydrogen-bonded complexes.

2. Experimental and computational methods

The crystals of $G_4Cl_2SO_4$ were obtained from the saturated aqueous solution of stoichiometric quantities of guanidinium carbonate $(H_2NC(=NH)NH_2)_2H_2CO_3$, sulfuric acid H_2SO_4, and hydrochloric acid HCl. From the obtained polycrystals the saturated water solution of the substance was prepared. Colorless and transparent crystals were grown by the slow evaporation method at constant temperature of 304 K.

The temperature dependent infrared spectra were measured with the resolution of 1 cm^{-1} in the range 4000–400 cm^{-1} by using a Nicolet Nexus FT-IR spectrometer with KBr windows. The samples were prepared as suspensions of powder obtained from the single crystals in Nujol mull. A Graseby–Specac variable-temperature cell was used to control the temperature. The measured sample temperature was changed in the range of 298–377 K on heating process first and then in the range of 377–313 K on cooling process. Each spectrum was assembled at constant temperature. The stability of the temperature was ±1 K. 128 scans were made and Fourier-transformed in order to obtain one spectrum. 128 spectra were co-added to improve the signal to noise ratio. In the FT-IR interferogram, when the cryostat was used, the zero path difference (ZPD) maximum fluctuated between $-2.2/-2.3$ at minimum and 5.6/5.2 at maximum. For the spectroscopic data analysis the multifunctional GALACTIC GRAMS/386 program was used. It is worth noting that the band positions obtained by curve fitting may slightly differ from the wavenumbers shown on the observed spectra.

A Bruker IFS66 spectrometer was used to record the FT–FIR spectra of the powdered $G_4Cl_2SO_4$ crystal in Nujol oil in the range of 600–50 cm^{-1} at room temperature (RT). The crystal in Nujol suspensions were placed between polyethylene windows. The spectrum in the range of 4000–400 cm^{-1} at room temperature (RT) was recorded with the use of the same Bruker IFS66 spectrometer. The sample was prepared as a compressed pellet made from powdered substances: $G_4Cl_2SO_4$ and KBr. The resolution was 1 cm^{-1}.

The Raman spectra of a powdered crystal at RT were recorded using a Nicolet Magna 860 FT-IR spectrometer, interfaced with a FT-Raman accessory. The Raman spectra were excited with a Nd:YVO_4 laser line at 1064 nm with a power of *ca.* 290 mW. The measurements were performed over the wavenumber range 3700–100 cm^{-1} with resolution of 4 cm^{-1}.

All calculations were performed with the Firefly (PC GAMESS) version 7.1.G, build number 5618 program [8], compiled under Linux operating system. This job was executed on small PC Cluster consisting of three server nodes with 32-bit and 64-bit AMD processors running at 1.8 GHz and 2 GB RAM. The MPICH [9] implementation of message passing interface (MPI) standard for communication between cluster nodes was used. This protocol ensures good performance and completes remote execution environment.

For calculation the structural data from X-ray investigations of crystal were used. The coordinates for particular atoms were established and the *Z*-matrix was built by Molden program [10]. The *Z*-matrix was directly used in input Firefly files. The optimized structures for all investigated forms of considered complex have been calculated by the DFT/B3LYP method. The 6-31++G(d,p) basis set has been employed. The harmonic frequencies and infrared intensities were calculated by the density functional triple parameter hybrid model (DFT/B3LYP) with identical basis set. The normal coordinate analysis has been carried out for investigated molecule according to the procedure described and recommended by Fogarasi and Pulay [11]. The all frequencies were scaled by 0.96 factor. The calculated potential energy distribution (PED) for the investigated molecule has enabled us to make detailed band assignment in infrared spectra.

3. Results and discussion

3.1. Vibrational spectra

3.1.1. Vibrational modes theory

The X-ray diffraction measurements [6] have shown that the crystal at room temperature is orthorhombic with the space group $Cmc2_1$ (C_{2v}^{12}) and $Z = 4$. The unit cell parameters at RT are: $a = 14.213(3)$ Å, $b = 9.474(5)$ Å, $c = 14.414(4)$ Å. Monovalent Cl^- and divalent SO_4^{2-} anions and G cations build two anionic sublattices [6]. The cations (signed as G(1), G(2), G(3) in [6]) occupy crystallographically different positions in

the structure. Due to the data [6] the anions SO_4^{2-} are located in the special positions so they are expected to occupy the Cs symmetry sites. Two of the four cations $[C(NH_2)_3]^+$ (G(2) and G(3)) also are placed in special positions on the mirror-symmetry plane.

The correlation diagram for these ions is presented in Table I. The diagram has been made on the basis of character tables [12]. In the unit cell $Z = 4$ [6] taking into account the crystal symmetry at RT, the number of formula units per the Bravais space cell $Z^B = 2$. Consider the cation symmetry in the unit cell, i.e. the factor group, it is easy to notice that the number of vibrations is multiplied by four.

TABLE I

Correlation table for the vibrational modes of $[C(NH_2)_3]_4Cl_2SO_4$; room temperature.

SO_4^{2-} molecular group: T_d	SO_4^{2-} site group: C_s	SO_4^{2-} factor group: C_{2v}	$[C(NH_2)_3]^+$ molecular group: D_{3h}	$[C(NH_2)_3]^+$ factor group: C_{2v}
A_1 (R)		4 A_1 (IR,R)	3 A_1' (R)	36 A_1 (IR,R)
	6 A' (IR,R)		2A_2'	
		A_2 (R)	6 E' (IR, R)	12 A_2 (R)
E (R)			A_1''	
	3 A'' (IR,R)	2 B_1 (IR,R)		16 B_1 (IR,R)
2F_2 (R, IR)			2A_2'' (IR)	
		2 B_2 (IR,R)		32 B_2 (IR,R)
			2E'' (R)	

IR – infrared active; R – Raman-active; the number of cationic internal vibrations in factor group have been multiplied by four.

The SO_4^{2-} free ions have a T_d symmetry. The irreducible representation for this symmetry is expressed as: $\Gamma_{\rm vib} = A_1(R) + E(R) + 2F_2(IR, R)$. All of the presented fundamental vibrational modes are Raman active and two triple degenerated are infrared active. Inside the crystal SO_4^{2-} ions have C_s site symmetry. The A' as well as A'' fundamental modes of the group both are infrared and Raman active.

The $[C(NH_2)_3]^+$ free ions have a D_{3h} symmetry, so the irreducible vibrational representation is expressed as: $\Gamma_{\rm vib} = 3A_1'(R) + 2A_2' + 6E'(IR, R) + A_1'' + 2A_2''(IR) + 2E''(R)$. Thus, eleven vibrational modes are the Raman active and eight vibrational modes are infrared active. In the crystal G cations are placed in different positions. G(2) and G(3) cations occupy special positions and G(1) cations are placed in general position [6]. Therefore no site symmetry for cations is presented in Table I.

The number of all the fundamental vibrational modes is equal to 135, while the number of fundamental modes presented in Table I amounts to 105. Only the modes which should be IR or Raman active have been included in the table.

3.1.2. IR spectra

The IR spectra in the range 4000–400 cm^{-1} measured for the crystal in Nujol mull at several temperatures during heating and cooling processes and in KBr at room temperature, and FT–FIR spectrum in the range of 600–50 cm^{-1} at room temperature are shown in Fig. 1. The band positions are marked for the most intense bands only in the curve which describes the outcomes of the spectrum at 313 K during heating run. In Fig. 1 a few groups of bands can be seen. In the high frequency range a very broad band from 3500 cm^{-1} to 2800 cm^{-1} is connected with NH_2 free symmetric and asymmetric and NH_2 bonded with hydrogen bonds stretching vibrations. In the range of 1750–1500 cm^{-1} the group of bands representing mainly NH_2 bending, but also CN stretching vibrations, can be seen. The next sharp band, with the maximum at 1098 cm^{-1} presents (SO_4^{2-}) stretching and NH_2 deformation vibrations. In low frequencies a broad group of bands spreads from 770 cm^{-1} to 400 cm^{-1}. The wavenumbers (the band positions of measured spectra), relative intensities and proposed detailed assignments of the internal vibrations in the crystal moieties, measured at 313 K, 356 K, and 377 K on heating and at 349 K and 113 K on cooling, are listed in Table II. The chosen temperatures correspond with the temperatures of the particular phase existence in the thermodynamic equilibrium in the crystal, on heating and cooling processes, respectively. The greatest changes of the band wavenumbers can be noticed for data in the first and the second column of the table, where the band positions at phases III and II are placed, respectively. Data in the third, fourth and the fifth column seems to be quite similar.

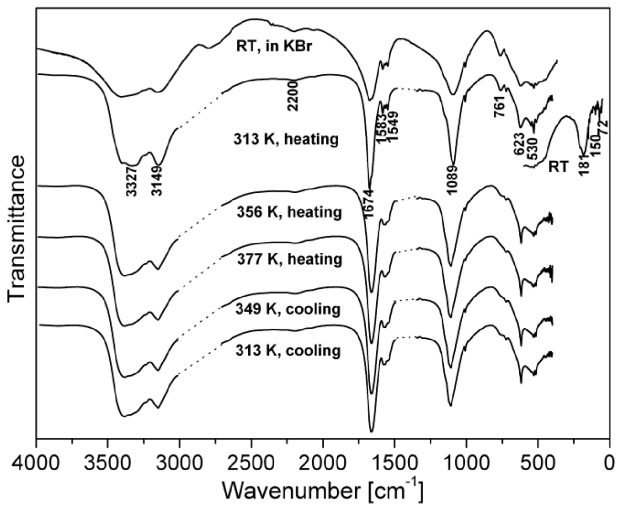

Fig. 1. The infrared spectra of $G_4Cl_2SO_4$ in Nujol mull measured in several phases at heating and cooling runs, the FT–FIR spectrum at room temperature and the IR spectrum in KBr at RT.

3.1.2.1. Temperature dependent spectra

Temperature detailed analysis and peak fitting to the obtained spectra were performed for these of the internal vibration bands, for which some significant temperature effects were observed. The effects were found especially at temperatures close to the temperature of the phase transitions. The studies show the noticeable changes of wavenumber, intensity, and gravity centre of the bands. Most of the sharp changes of these parameters occur between the two successive measured temperatures: 356 K and 358 K taken after four hours. So, the middle temperature of 357 K has been adopted as the PT temperature.

TABLE II

Experimental data (IR and FT–FIR (*) in Nujol medium; FT–FIR, Raman and in KBr pill (**) at room temperature; Raman on powder) for $G_4Cl_2SO_4$; (***) — after four hours at 356 K; vs — very strong; s — strong; m — medium; w — weak; vw — very weak; sh — shoulder; Band — frequency in cm^{-1}; I — intensity; h — heating; c — cooling.

IR						Raman		Assignment
313 K^h band	356 K^{h***} band	377 K^h band	349 K^c band	313 K^c band	I	303 K band	I	
3405	3384	3384	3384	3387	s			
						3340	w	
3327	3334	3334	3334	3334	s			$\nu_{as}(NH_2)$
3295	3291	3291	3285	3289	s			$\nu_s(NH_2)$
						3268, sh	vw	
3237	3233	3233	3233	3233	s			
						3179	vw	$\nu(NH_2)$ bonded
3149	3150	3150	3150	3150	s			
2795**								
2723**, sh								
2200	2194	2190	2194	2196	vw			overtone
2079	2079	2079	2079	2079	vw			
2057sh					vw			
1674	1661	1661	1661	1661	vs			$\delta(NH_2) + \nu_{as}(CN)$
1660					vs			
						1644	w	
1583					w			
	1579, sh		1577, sh	1579	w			
					w	1568	w	$\delta(NH_2)$
1566	1567	1567	1566	1566	w			
1549	1549	1553	1548	1548	w			
	1539	1539	1539	1538	w			
1180, sh	1179, sh	1179, sh	1179, sh	1179, sh	vw			$\nu_{as}(CN)$
1151, sh	1149, sh	1149, sh	1147, sh	1147, sh	w			
1106, sh	1122	1122	1122	1122	s			$\gamma(NH_2) + \nu_{as}(SO_4^{2-})$, (ν_3)
1089	1108	1108	1108	1108	s			
1008	1007	1006	1007	1007	w	1010	vs	$\nu_s(CN)$
1005					w			
979	983, sh	983, sh	983	983	vw			$\nu_s(SO)$, (ν_1)
	979, sh		979, sh		vw	979	m	
761	764, sh		758, sh	762, sh	w			
	624, sh	624, sh	624, sh	624, sh	m	621	w	$\delta_s(SO_4^{2-})$, (ν_2)
623	618	618	618	618	m			
549					m			
536, sh							m	
530	531	531	531	531	m	532	m	$\delta(CN)$
512	516	516	516	516	m			
468, sh					m			$\omega(NH_2) + \delta_{as}(SO_4^{2-})$, (ν_4)
450					m	454	w	
206*					m			
181*					m			$\nu(CN)$
171*					m			
150*					m			Lattice vibrations
100*					vw			
72*					vw			Lattice vibrations

The most interesting temperature effects in the infrared spectra were observed in the range of 1750–1500 cm^{-1}. Figure 2a presents bands in this frequency interval, assigned to $\delta(NH_2)$ and $\nu(CN)$ vibrations at several temperatures. At 313 K five distinct bands can be noticed at 1674, 1660, 1583, 1566, and 1549 cm^{-1} whereas at 356 K one non split band at 1661 cm^{-1} has been found and a few poorly split bands at 1567, 1549,

1539, and a shoulder at 1579 cm^{-1}. Temperature dependence of the fitted band frequencies in the range mentioned above is presented in Fig. 2b. The frequency changes can be noticed near the temperatures of 352 K and 358 K, respectively. These temperatures are close to the temperatures of the phase transitions. The temperature dependence of the fitted mode at 1640 cm^{-1} position is presented in Fig. 2c. (The position of a fitted mode may differ a little from its position in experimental spectrum.) The position of the mode gradually shifts to lower frequencies with temperature increasing. The changes seem to be larger when the temperature approaches 352 K that is to the range of the coexistence of two phases, III and II, observed in the temperature range 352–357 K [7].

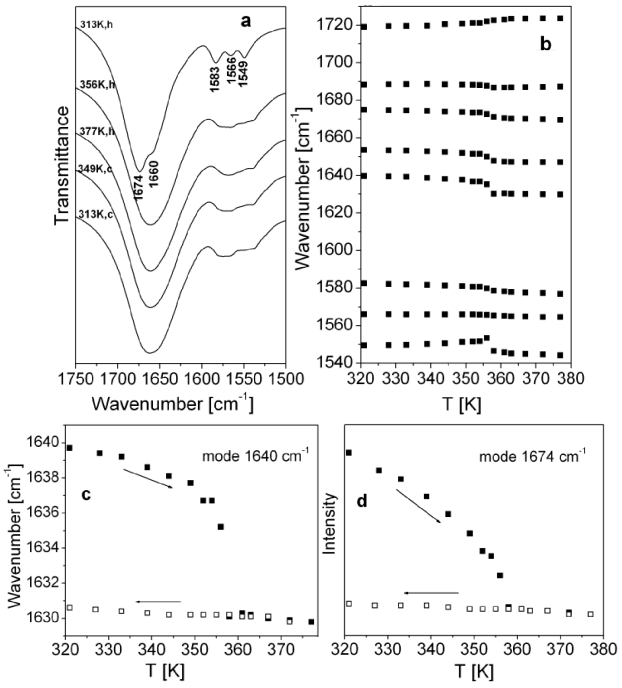

Fig. 2. (a) Temperature evolution of the IR spectra of $G_4Cl_2SO_4$ crystal in the range of 1750–1500 cm^{-1} (the frequency range assigned to bending NH_2 vibrations and stretching CN vibrations) at several temperatures; h — heating, c — cooling; (b) temperature dependence of wavenumbers of bands fitted in the range mentioned above; (c) temperature dependence of the fitted mode at 1640 cm^{-1} position; (d) the temperature evolution of the NH_2 mode at 1674 cm^{-1} intensity. Arrows indicate heating and cooling processes.

The rapid shift can be seen near the temperature of the phase transition, i.e. 357 K. What is noteworthy, the rapid changes of the mode positions have been observed only in the heating process, while on cooling process the changes have been very slight. The temperature evolution of the bending NH_2 mode at 1674 cm^{-1} intensity is presented in Fig. 2d. The peak intensity is nonlinearly diminishing during heating and the most intense changes are observed near the 357 K, i.e. the PT temperature. Above this temperature the mode intensity is almost stable. On cooling process the mode intensity is nearly stable in the whole temperature range 380–298 K.

In Fig. 2a the band at 1674 cm^{-1} displacement can be seen towards lower frequencies together with the increase in temperature (i.e. shift towards higher frequencies with temperature decreasing) till 357 K. The band at 1674 cm^{-1} at RT has been assigned to the $\delta(NH_2)$ vibrations. Similarly, the fitted band at 1640 cm^{-1} displacement can be seen in Fig. 2c.

As shown in [13], a formation of A–H ... B complexes causes a shift of the δ(A–H) vibrations towards higher frequencies. In Fig. 2a–c the bands shift in the opposite direction, i.e. towards lower frequencies with the increase in temperature can be seen. Thus, according to [13], the weakening of N–H ... O hydrogen bonds when the temperature increases till PT temperature have been observed in the $G_4Cl_2SO_4$ crystal. At about 357 K due to the disappearance of phase III the position of the mode at 1640 cm^{-1} shifts rapidly from 1635 cm^{-1} to 1630 cm^{-1} (Fig. 2c). Thus, the phase transition III–(II)I is connected with the weakening of the N–H ... O hydrogen bonds. It is in good agreement with the structural data [6]. In phase I, in temperatures above 357 K, the band position changes are insignificant.

All the effects discussed so far concern $[C(NH_2)_3]^+$ cations. Another range with the noticeable changes of temperature measured spectra is the range of 950–1200 cm^{-1}, which contains bands connected with both the anion and cation vibrations. Spectra obtained in this wavenumber range are presented in Fig. 3a. The bands have been assigned to $\gamma(NH_2)$ and $\nu(SO_4^{2-})$ vibrations. Some kind of the isosbestic point can be seen in this figure at 1108 cm^{-1}. In UV–VIS spectroscopy, an isosbestic point is a specific wavelength at which two chemical species have the same molar absorbance. More generally, an isosbestic point is a specific wavelength at which two chemical species are linearly related. The isosbestic points theory is described in [14].

The bands presented in Fig. 3a cross in the point at 1108 cm^{-1}. The bands with the transmittance minimum at 1089 cm^{-1} are connected with the ferroelectric phase, while the bands with the transmittance minimum at 1108 cm^{-1} — with the paraelectric one.

The temperature dependence of the maximum peak position in the frequency range mentioned above is presented in Fig. 3b. It is evident that on heating till 330 K the mode position is almost stable and then it starts to move linearly towards higher wavenumbers. The changes of the mode at 1089 cm^{-1} position indicate a release of SO_4^{2-} motion below the PT temperature. Then, at 357 K the maximum position changes rapidly. At temperatures above the PT the position of the maximum is almost stable. On cooling run the maximum position does not change in the whole temperature range. The temperature dependence of the intensity of the mode at 1089 cm^{-1} is presented in Fig. 3c. The intensity is nonlinearly and

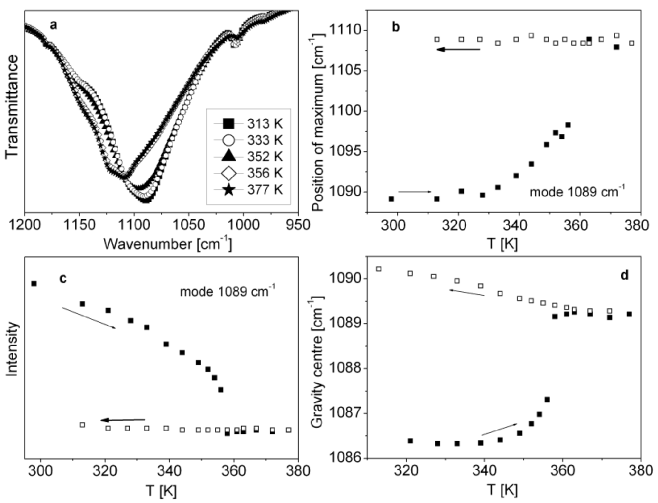

Fig. 3. (a) Transmittance measured at the range of 950–1200 cm^{-1} (the frequency range assigned to $\gamma(NH_2)$, $\nu(SO_4^{2-})$ and $\nu(CN)$ groups) for several temperatures; (b) temperature dependence of the position of maximum in this spectral range; (c) temperature dependence of the mode at 1089 cm^{-1} intensity; (d) temperature dependence of the gravity centre position. Arrows indicate heating and cooling processes.

slightly diminishing during the increase in temperature and at 357 K the jump of the peak intensity towards smaller values is observed. At higher temperatures, as well as on cooling process the intensity is almost at the same level.

Figure 3d presents the temperature dependence of the gravity centre position on cooling and heating. The definition of the gravity centre (i.e. the first spectral moment) was presented in [15, 16]:

$$M^{(1)} = \frac{\int A_\nu \nu \, \mathrm{d}\nu}{\int A_\nu \, \mathrm{d}\nu},$$

where $M^{(1)}$ is the centre of gravity of the band in cm^{-1}, A_ν is the absorbance and ν is the wavenumber in cm^{-1}.

One can see that on heating the position of the gravity centre is almost stable with temperature till 350 K. Above this temperature the gravity centre position shifts gradually to higher frequencies. The temperature range 352–357 K corresponds to the range of the coexistence of two phases, III and II, described in [7]. The displacement of about 2 cm^{-1} towards higher frequencies can be noticed at 357 K. Above this temperature the gravity centre position is almost stable with the temperature again. The movement towards higher frequencies indicates the weakening of SO_4^{2-} and N–H . . . O bonds, which is in accordance with the structural data [6]. On cooling the gravity centre position shifts insignificantly to higher frequencies.

Thus, the cationic and anionic dynamics contribution to the phase transition mechanisms in $G_4Cl_2SO_4$ crystal was proved.

3.1.2.2. Time dependent spectra

Taking the temperature spectra changes and the coexistence of phases III and II [7] into consideration time dependent spectra were measured. The sample was heated till 356 K and at this temperature the IR spectra were taken during a few hours. Figure 4a presents time evolution connected with the slow transition from the phase III to II observed in the spectral range 1750–1500 cm^{-1} at 356 K (compare with Fig. 2a). The changes in the spectra are remarkable. The mode at 1665 cm^{-1} on the upper curve is shifted to the position of 1660 cm^{-1} on the curve measured after 214 min. After that time the position of the mode is almost stable. Another changes can be noticed in the range 1600–1500 cm^{-1}. Three very well separated bands are seen in this range on the upper curve, whereas on the bottom curve the bands are not well separated. The bands in the spectral range 1600–1530 cm^{-1} after 1 and 242 min, respectively, are shown in the inset of Fig. 4a. On the upper curve three bands appear, at 1583, 1566, and 1549 cm^{-1}, while on the bottom curve a few poorly split bands at 1567, 1549, 1539, and a shoulder at 1579 cm^{-1} can be found. Moreover, the intensity of the band at 1583 cm^{-1} diminishes and the band broadens, a new weak band at 1548 cm^{-1} appears, the band at 1548 cm^{-1} shifts at about 10 cm^{-1} to 1539 cm^{-1} position.

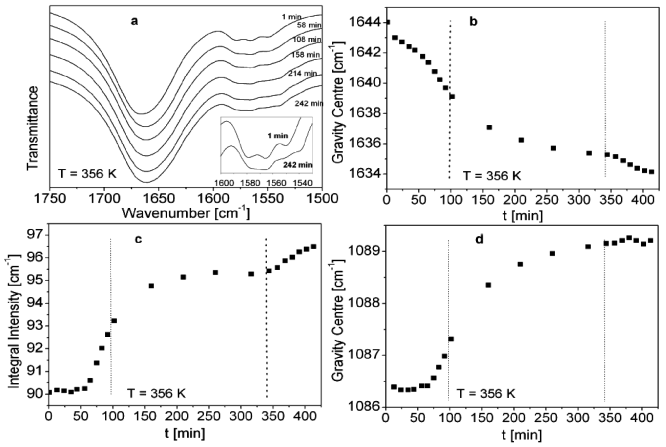

Fig. 4. (a) The infrared spectra of $G_4Cl_2SO_4$ crystal in the range of 1750–1500 cm^{-1} at constant temperature of 356 K, measured in several times; (b) time evolution of the gravity centre (in this spectral range) position; (c) time dependence of integral intensity of this spectral range; (d) time evolution of the gravity centre for bands in the range 950–1200 cm^{-1}. Dashed, vertical line indicates the time interval when the sample temperature was constant.

Figure 4b shows time dependence of the gravity centre for the spectral range 1750–1500 cm^{-1}. The points, which occur between the two vertical lines show the time range, where the crystal was kept at constant temperature. One can see that the position of the gravity centre shifts gradually to lower frequencies with time and then,

at constant temperature it starts to stabilize. Such a dependence shows that the changes are connected with slow transition III → II, and the coexistence of the phases, which is in accordance with the data in [7]. After the stabilization, behind the second vertical line, in phase I, the gravity centre position shifts slightly towards lower wavenumbers together with the temperature changes. Figure 4c presents integral intensity time dependence of the discussed range. At constant temperature integral intensity shifts to higher frequencies and then, at about time of 200 min it does not change.

Figure 4d shows time dependence of the gravity centre for the frequency interval of anionic vibrations, as in Fig. 3a. One can see that the position of the gravity centre shifts gradually to higher frequencies with time and then, after about 320 min, it poorly changes its position. Then, when the crystal rests in phase I, despite heating, the gravity centre almost does not change the position.

Figure 4b–d points out that the phase II appears before the temperature was stopped at 365 K. In the time range, where the temperature is constant, at first the observed spectral parameters changes point at the coexistence of phases III and II. Then, after about three hours, the changes of the presented parameters start to be very slight and one can assume that only phase II exists in the crystal. Then, on heating, the phase transition II–I takes place, which is almost invisible in the spectra.

So, the differences in the time dependent spectra can be remarkably distinguished and the changes are resulting from the observed transition between III and II phases. After four hours, the changes are not observed as the transition to phase II is completed.

3.2. Raman spectra

Raman spectrum in the range 3700–100 cm^{-1} at room temperature is shown in Fig. 5. The band frequencies of the Raman spectrum, their intensities and the proposed assignments of the internal vibrations are placed in the seventh, eighth and ninth column of Table II. It has been known from the structural methods and character tables that $4A_1$, $1A_2$, $2B_1$, and $2B_2$ anionic and $36A_1$, $12A_2$, $16B_1$, and $32B_2$ cationic vibrational modes should be Raman active. The theoretical active Raman vibrational modes are listed in Table I.

The most intense internal vibration band in Fig. 5 is the band at 1010 cm^{-1} and it is assigned to stretching symmetric vibration of CN group. In the spectral range 3700–1010 cm^{-1} only several very weak Raman bands can be seen and they are assigned to $\nu(NH_2)$, $\delta(NH_2)$, and $\nu(CN)$ vibrations, respectively. In the range 1010–100 cm^{-1} only four bands at *ca.* 500 cm^{-1} can be distinguished, some of them of the weak intensity. The bands at 979, 621, and 454 cm^{-1} are assigned to $\nu(SO_4^{2-})$ vibrations and are named as ν_1, ν_4, and ν_2 modes, respectively [17, 18]. According to [19] the existence of all the ν_1, ν_2, ν_3, and ν_4 bands of SO_4^{2-} ion at IR spectrum and ν_1, ν_2, and ν_4 bands in Raman spectrum indicates a lowering of symmetry from T_d to C_s, which is consistent with the crystallographical data [6].

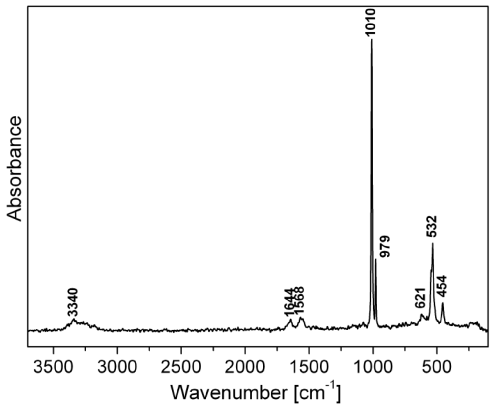

Fig. 5. Raman spectrum of the crystal at room temperature.

In accordance with the theory fewer bands is Raman active than IR active. There are only two bands, at 1010 cm^{-1}, 979 cm^{-1}, which are active both in IR and Raman spectra. A lot of bands measured experimentally, which are IR active or Raman active, have their frequencies shifted over a few cm^{-1}.

3.3. DFT calculations

3.3.1. IR calculated spectra

Isolated $[C(NH_2)_3]_4Cl_2SO_4$ molecule has been optimized by using the DFT/B3LYP method. The 6-311++G(d,p) basis set has been employed. The obtained conformation is presented in Fig. 6. The energy of the conformation is $E = -2440$ kcal/mol $= -10211$ kJ/mol. The main reasons for the singling out of the isolated molecule is the same stoichiometric composition as for the isolated $G_4Cl_2SO_4$ molecule, i.e. it consists of four $[C(NH_2)_3]^+$ cations, one SO_4^{2-} anion and two Cl^- anions in spite of that the number of molecules per unit cell in the real crystal is 4.

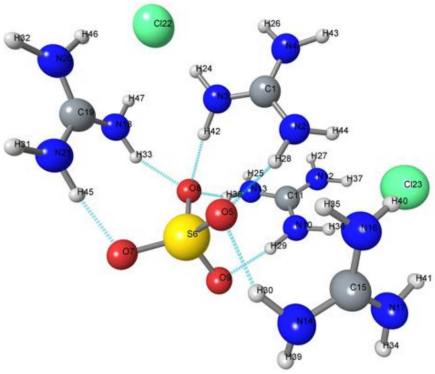

Fig. 6. Calculated structure of $[C(NH_2)_3]_4Cl_2SO_4$ molecule in gas environment. Hydrogen bonds N–H ... O have been signed.

There are several hydrogen bonds in the calculated molecule. Not all of the hydrogen bonds are presented in Fig. 6, but all of them are listed in Table III. The detailed

TABLE III

Hydrogen bond parameters in calculated conformation of $G_4Cl_2SO_4$.

Hydrogen bond	D–H [Å]	A . . . H [Å]	D–A [Å]	Angle [°]
N3–H42 . . . O8	1.050	1.694	2.712	161.914
N18–H33 . . . O8	1.055	1.651	2.682	164.390
N13–H38 . . . O8	1.061	1.622	2.667	167.203
N21–H45 . . . O7	1.070	1.58	2.629	164.640
N14–H30 . . . O5	1.042	1.781	2.726	148.882
N2–H28 . . . O5	1.079	1.540	2.619	179.025
N16–H35 . . . O5	1.046	1.769	2.723	149.673
N10–H29 . . . O9	1.071	1.566	2.632	172.867
N17–H34 . . . Cl23	1.046	2.192	3.150	151.453
N14–H39 . . . Cl23	1.035	2.315	3.224	145.792
N3–H24 . . . Cl22	1.034	2.319	3.228	145.889
N4–H26 . . . Cl22	1.040	2.301	3.230	147.981

D — donor; A — acceptor.

description of the hydrogen bonds presented in Fig. 6 is as follows: one SO_4^{2-} anion is linked to $[C(NH_2)_3]^+$ surrounded cations by eight N–H . . . O hydrogen bonds. One oxygen atom (O7 in Fig. 6) is single hydrogen bonded with NH hydrogen atom from one $(NH_2)_3$ group. The second oxygen atom (O8) is bonded with three-furcated NH hydrogen bonds from three different $C(NH_2)_3$ groups. Next of the O atoms (O5 in Fig. 6) is connected to the neighboring guanidinum cation by a three-furcated NH hydrogen bonds from the two different $C(NH_2)_3$ groups. The last oxygen atom (O9) is single hydrogen bonded with NH hydrogen atom from one $C(NH_2)_3$ group, i.e. N10–H29 . . . O9. The N–O distances differ from 2.619 Å to 2.726 Å. The average distance D–A (donor–acceptor) is equal to 2.674 Å. That is a little less than in the real crystal, where the D–A distance on average was equal to 2.901 Å [6]. In calculated conformation the SO_4^{2-} anion is tied by hydrogen bonds more strongly than in crystal.

In Table III N–H . . . Cl bonds are presented. Each chlorine anion is connected with a bifurcated hydrogen bond with NH hydrogen atom. Each of hydrogen bonds in bifurcated hydrogen bond ties Cl anion and NH nitrogen atom from the same $C(NH_2)_3$ group. The N–Cl distances differ from 3.150 Å to 3.230 Å. The average distance D–A is equal to 3.208 Å. That is a little less than in the real crystal, where the D–A distance on average was equal to 3.390 Å [6]. In calculated conformation the Cl^- anions are tied by hydrogen bonds stronger than in real crystal. The N–H . . . Cl bonds are strongly bent.

The frequency, scaled frequency, band intensity, and the proposed assignments of the calculated internal vibrations are presented in Table IV (at the end of paper). The calculated potential energy distribution (PED), which is included in the fourth column of Table IV was the basis of the clear assignment of the bands. There are 3N-6, i.e. 135 bands (lines) in the table. Comparison of the wavenumbers and intensities of conformation calculated bands and experimental crystal bands shows very good conformity. Theoretical spectrum of $G_4Cl_2SO_4$ molecule is presented in Fig. 7.

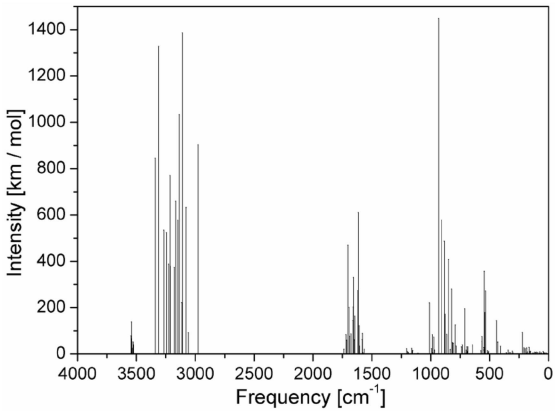

Fig. 7. Theoretical B3LYP-calculated IR frequencies of $G_4Cl_2SO_4$ crystal.

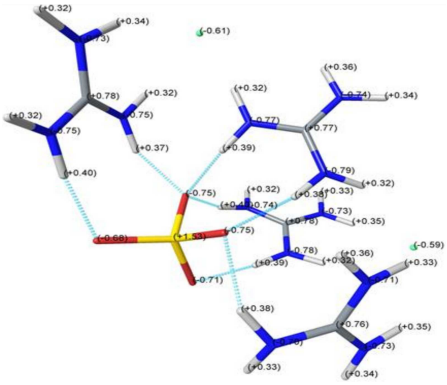

Fig. 8. Arrangement of the Mulliken charges calculated for $[C(NH_2)_3]_4Cl_2SO_4$ conformation.

The three groups of intense bands can be noticed in Fig. 7. One of them occurs in the frequency range of 3348 cm^{-1} to 2969 cm^{-1} and is assigned to antisymmetric and symmetric NH_2 vibrations. The other group of bands possessing the intensity lower than the group mentioned above, extends from 1734 cm^{-1} to 1553 cm^{-1}. This frequency interval is assigned mostly to bending NH_2 and stretching CN vibrations. The third group of bands with high intensity in Fig. 7 occurs in the frequency range of 1018 cm^{-1} to 442 cm^{-1} and is assigned to bending NH_2, bending CN vibrations, among others. Similar assignment can be found in table with experimental data (Table II).

Consider that the conformation in gas is not comparable with the real crystal structure and bonding, the theoretical results correspond to experimental findings. This way, the theoretical bands can be compared with experimental ones.

3.3.2. Mulliken charges analysis

The Mulliken population analysis was performed by density functional method with the use of the 6-311++G(d,p) basis set. The arrangement of the Mulliken charges calculated for $[C(NH_2)_3]_4Cl_2SO_4$ confor-

mation is presented in Fig. 8. It is evident that the total charge of anions and cations is not localized, but is disturbed among all the atoms. Hydrogen atoms charges in G cations slightly differ from one another ($+0.32e \div +0.40e$). Two oxygen atoms (O5 and O8, respectively) have the same charges ($-0.75e$) and the other two differ with their charges. The S–O bond lengths which come out from the theoretical calculations are as follows: the distances S6–O5 and S6–O8 are equal to 1.679 Å; the distance S6–O7 amounts to 1.611 Å and the distance S6–O9 amounts to 1.616 Å. It is easy to notice that the oxygen atoms with the same S–O bond lengths have the same charges.

The information in Figs. 6 and 8 shows very well the possibility of the distinction between single and double bond in the sulphuric acid. It is noteworthy that the hydrogen atoms which form N–H ... O hydrogen bonds, have a little higher charges with comparison to the other hydrogen atoms in guanidine cations. That may be a result of the hydrogen bond construction. Two Cl^- anions have comparable charges ($-0.61e$ and $-0.59e$, respectively).

4. Summary

Wide temperature range vibrational analyses have been performed for the tetraguanidinium dichloro-sulfate crystal. A detailed analysis of frequencies, intensities and gravity centre position of the bands has been done. Significant changes of the parameters have been distinguished especially at temperatures close to the temperatures of the PTs. The special attention was paid on the phase II, whose appearance is time dependent. Time dependent spectra at constant temperature were measured and analysed. Similarly the room temperature Raman spectra were examined. Theoretical calculations of vibrational spectra were performed. The Mulliken charge analysis was done. On the basis of the results the final conclusions have been stated:

1. The spectra evidence phase transition III–II on heating, coexistence of phases III and II, and slow kinetics in the temperature range 352–357 K. There is no clear evidences of the transition II–I on heating and I–II on cooling at 354 K.

2. Changes in the IR spectra at 357 K for modes connected with both the guanidinium cations and sulfate anions (1750–1500 cm^{-1} and 1240–860 cm^{-1}, respectively) clearly indicate to the contribution of anions as well as cations to the mechanism of phase transitions in $G_4Cl_2SO_4$ crystal.

3. The phase transition III–I (through the phase II) has been connected with the weakening of the N–H ... O hydrogen bonds.

4. The IR and Raman spectra point at the lowering of both the T_d anion symmetry and D_{3h} cation symmetry in the crystal.

5. The B3LYP-calculated frequencies show good agreement with experimental data.

6. The asymmetric charge distribution confirms the symmetry lowering inside the crystal obtained from the experimental method.

References

[1] C.L. Angell, N. Sheppard, *Trans. Faraday Soc.* **53**, 589 (1957).

[2] M. Drozd, *Mater. Sci. Eng. B* **136**, 20 (2007).

[3] M. Drozd, J. Baran, A. Pietraszko, *Spectrochim. Acta, Part A* **61**, 27 (2005).

[4] M. Drozd, *Spectrochim. Acta, Part A* **69**, 1223 (2008).

[5] M. Drozd, J. Baran, *Spectrochim. Acta, Part A* **61**, 2953 (2005).

[6] M. Szafrański, *Phys. Rev. B* **72**, 054122 (2005).

[7] A. Rokosa, Z. Czapla, S. Dacko, B. Kosturek, *J. Phys. Chem. Sol.* **74**, 7 (2013).

[8] A. Granovsky, Firefly version 7.1.G, `classic.chem.msu.su/gran/firefly/index.html` .

[9] RWTH Aachen, *Lehrstuhl fuer Betribssysteme*, 2005.

[10] G. Schaftenaar, J.H. Noordik, *J. Comput.-Aided Mol. Design* **14**, 123 (2000).

[11] G. Fogarasi, P. Pulay, in: *Vibrational Spectra and Structure*, Vol. 13, Eds. J.R. During, Elsevier, New York 1985.

[12] W.G. Fateley, F.R. Dollish, N.T. McDevitt, F.F. Bentley, *Infrared and Raman Selection Rules for Molecular and Lattice Vibrations: The Correlation Method*, Wiley, New York 1972.

[13] S. Schroetter, D. Bougeard, *Ber. Bunsenges. Phys. Chem.* **91**, 1217 (1987).

[14] D.M. Cohen, E. Fischer, *J. Chem. Soc.*, 3044 (1962).

[15] V.E. Borisenko, Yu.A. Zavjalova, T.G. Tretjakova, Z.S. Kozlova, A. Koll, *J. Mol. Liq.* **109**, 125 (2004).

[16] D. Podsiadła, O. Czupiński, M. Rospenk, Z. Czapla, *Vibrat. Spectrosc.* **55**, 160 (2011).

[17] H.H. Adler, P.F. Kerr, *Am. Mineral.* **50**, 132 (1965).

[18] R.L. Frost, R. Scholz, A. López, Y. Xi, *Spectrochim. Acta A* **116**, 165 (2013).

[19] J.T. Kloprogge, D. Wharton, L. Hickey, R.L. Frost, *Am. Mineral.* **87**, 623 (2002).

TABLE IV

Calculated (B3LYP/6-311++G(d,p)) IR spectral data for $G_4Cl_2SO_4$.

Frequency [cm^{-1}]	Scaled frequency [cm^{-1}]	Intensity [km/mol]	PED % (more than 10%)	*A*
3 694	3 547	79	N20–H32 95	ν_{as}NH
3 693	3 545	50	N12–H27 93	ν_{as}NH
3 690	3 542	138	N17–H41 86	ν_{as}NH
3 688	3 541	65	N4–H43 96	ν_{as}NH
3 685	3 538	25	N16–H40 88	ν_{as}NH
3 679	3 531	52	N21–H31 97	ν_{as}NH
3 676	3 529	52	N13–H25 97	ν_{as}NH
3 672	3 525	40	N2–H44 98	ν_{as}NH
3 480	3 341	844	N14–H30 66, N14–H39 26	ν_{as}NH
3 448	3 310	1 328	N3–H24 70, N3–H42 11	ν_{as}NH
3 404	3 268	534	N10–H36 50, N12–H37 26, N14–H30 10	ν_sNH
3 379	3 244	524	N18–H47 51, N3–H24 15, N18–H33 15, N20–H46 14	ν_{as}NH
3 360	3 226	388	N14–H39 32, N10–H36 16, N16–H35 13	ν_{as}NH
3 349	3 215	770	N20–H46 28, N12–H37 20, N14–H39 15, N18–H33 14	ν_sNH
3 346	3 213	379	N12–H37 42, N20–H46 19, N10–H36 16	ν_{as}NH
3 310	3 177	374	N3–H42 33, N16–H35 16, N20–H46 13	ν_sNH
3 298	3 166	660	N16–H35 57, N3–H42 17	ν_sNH
3 279	3 148	576	N17–H34 72, N14–H39 11	ν_sNH
3 267	3 137	1 033	N18–H33 26, N18–H47 21, N4–H26 16, N21–H45 13	ν_sNH
3 244	3 114	222	N4–H26 54, N3–H42 15, N18–H33 12	ν_sNH
3 238	3 109	1 386	N10–H29 44, N13–H38 23	ν_sNH
3 208	3 079	632	N21–H45 76, N18–H33 12	ν_sNH
3 184	3 057	92	N13–H38 59, N10–H29 32	ν_sNH
3 100	2 976	903	N2–H28 94	ν_sNH
1 810	1 737	21	C19–N18–H47 20, C1–N3–H24 16, C1–N3–H42 16, C19–N18–H33 15	δNH
1 792	1 721	84	C11–N13–H38 39, C11–N13–H25 14, C11–N10–H29 11, C11–N10–H36 11, C11–N12–H37 10	δNH
1 786	1 714	59	C1–N2–H28 31, C19–N18–H47 10, C1–N2–H44 10	δNH
1 776	1 705	469	C19–N21–H45 27, C1–N2–H28 11	δNH
1 765	1 694	201	C15–N16–H35 32, C15–N17–H34 25	δNH
1 759	1 689	77	C11–N10–H29 29, C11–N10–H36 28, C11–N13–H38 16, N10–C11 12	δNH, νCN
1 747	1 677	87	C1–N3–H42 17, C1–N3–H24 14, C19–N18–H47 14, C19–N18–H33 12, C1–N2–H28 12, C19–N21–H45 10	δNH
1 730	1 661	145	C11–N12–H37 44, C11–N12–H27 16, C11–N13–H25 12	δNH, νCN
1 728	1 658	202	C19–N20–H46 24, C1–N4–H26 18, C19–N20–H32 10, C19–N21–H31 10	δNH
1 725	1 656	330	C15–N14–H39 32, C15–N14–H30 21, N14–C15 18	δNH, νCN
1 717	1 649	61	C1–N4–H26 30, C19–N20–H46 18, C1–N4–H43 12	δNH
1 715	1 646	163	C15–N17–H41 20, C15–N17–H34 18, C15–N16–H35 17, C15–N16–H40 14	δNH, νCN
1 686	1 618	273	C1–N2 13	νCN
1 682	1 615	611	C15–N16 13, C15–N17 11	νCN
1 674	1 607	122	C11–N13 31, C11–N10–H36 14, N10–C11 13, C11–N12–H27 12	νCN, δNH
1 672	1 605	34	C1–N2 17, C19–N21 17	νCN
1 649	1 583	62	C11–N12 22, C11–N10–H29 18, N10–C11 17, C11–N13–H25 11, C11–N12–H27 11	νCN, δNH
1 648	1 582	89	C19–N20 15, C19–N18–H33 13, N18–C19 11, C1–N3 10	νCN, δNH
1 640	1 575	4	C1–N3 19, C1–N4–H43 13, C1–N4 11, C1–N2–H44 10	νCN, δNH
1 631	1 565	21	N14–C15 23, C15–N16–H40 20, C15–N17–H41 20, C15–N14–H39 13, C15–N14–H30 11	νCN, δNH
1 255	1 205	23	C1–N3–H42 28, C1–N3–H24 27, C1–N2 11	γNH, νCN
1 247	1 197	10	C11–N10–H36 33, C11–N10–H29 33, C11–N13 17	γNH, νCN
1 244	1 194	2	C15–N14–H30 32, C15–N14–H39 31, C15–N17 17, C15–N16 14	γNH, νCN

TABLE IV — cont.

Frequency [cm^{-1}]	Scaled frequency [cm^{-1}]	Intensity [km/mol]	PED % (more than 10%)	*A*
1 241	1 191	7	C19–N18–H33 28, C19–N18–H47 26, C19–N21 13	γNH, νCN
1 209	1 161	24	C1–N2–H44 25, C1–N3 16, C1–N2–H28 16	γNH, νCN
1 209	1 160	20	C11–N13–H25 26, N10–C11 18, C11–N13–H38 16, C11–N12–H37 11	γNH, νCN
1 203	1 155	11	C19–N21–H31 21, N18–C19 19, C19–N21–H45 15, C19–N20–H46 12, C19–N20–H32 12	γNH, νCN
1 201	1 153	15	C15–N16–H40 21, N14–C15 20, C15–N16–H35 19, C15–N17–H41 11, C15–N17–H34 10	γNH, νCN
1 160	1 114	2	C1–N4–H43 39, C1–N4–H26 21, C1–N2–H44 20	γNH
1 152	1 106	1	C11–N12–H27 35, C11–N13–H25 23, C11–N12–H37 21, C11–N13–H38 10	γNH
1 150	1 104	2	C15–N17–H41 36, C15–N16–H40 22, C15–N17–H34 20, C15–N16–H35 11	γNH
1 147	1 101	1	C19–N20–H32 33, C19–N21–H31 26, C19–N20–H46 18, C19–N21–H45 12	γNH
1 053	1 011	221	N3–C1–N2–H28 21, N21–C19–N18–H33 17, N4–C1–N3–H42 11	ωNH
1 034	993	23	N13–C11–N10–H29 19, C11–N13 14, C11–N12 12	$\nu_s CN_{(breathe)}$, ωNH
1 028	987	83	C15–N17 16, C15–N16 16, N14–C15 15, C11–N12 11, C11–N13 10	$\nu_s CN_{(breathe)}$
1 025	984	4	C19–N20 25, C19–N21 22, N18–C19 18	$\nu_s CN_{(breathe)}$
1 014	974	73	C1–N4 16, C1–N3 15, C1–N2 14	$\nu_s CN_{(breathe)}$, ω NH
1 006	966	17	N13–C11–N10–H29 20	ωNH
973	934	1 448	N3–C1–N2–H28 48, N21–C19–N18–H33 13	ωNH
946	908	577	N14–C15–N16–H35 21, S6–O9 16, S6–O7 15	ν_{as}SO, ωNH
921	884	487	N17–C15–N14–H39 22, N14–C15–N17–H34 16, S6–O7 13	ωNH, ν_{as}SO
916	879	171	N14–C15–N16–H35 17, N21–C19–N18–H33 16, N4–C1–N3–H24 16, N20–C19–N21–H45 14, N3–C1–N4–H26 12	ωNH,
901	865	85	S6–O7 13, N17–C15–N14–H39 12, N14–C15–N16–H35 11	ν_{as}SO, ρNH
884	849	408	N4–C1–N3–H42 25, N21–C19–N20–H46 12	ρNH
868	833	19	N12–C11–N13–H38 27, N20–C19–N21–H45 15, S6–O7 12	ρNH, ν_sSO
858	823	281	N14–C15–N17–H34 31, N13–C11–N10–H36 18, N13–C11–N12–H37 11	ρNH
849	815	49	N21–C19–N18–H47 26, N3–C1–N4–H26 24, N20–C19–N21–H45 20, N4–C1–N3–H24 11	ρNH
841	808	47	S6–O9 27, N17–C15–N14–H30 17	ν_sSO, ρNH
826	793	125	N17–C15–N14–H30 27, N14–C15–N16–H35 11	ρNH
818	786	34	N3–C1–N4–H26 25, N4–C1–N3–H42 20, N21–C19–N18–H33 18	ρNH
771	740	30	N4–C1–N3–H24 18, S6–O8 17, N21–C19–N20–H46 16, O5–S6 12, N3–C1–N4–H26 11	δSO, ρNH
764	733	40	N14–C15–N17–H34 28, N17–C15–N14–H39 23, N17–C15–N14–H30 12	ρNH
739	710	195	S6–O8 23, O5–S6 21, N21–C19–N20–H46 10	δSO, ρNH
729	700	3	N3–N2–C1–N4 26, N13–C11–N10–H36 16	ρNH
727	698	17	N3–N2–C1–N4 58	δCN
717	688	11	O8–N18–C19–N21 51, N3–N2–C1–N4 21, N21–C19–N20–H46 18, O8–N18–C19–N20 12	δCN
721	692	30	O9–N14–C15–N17 39, O9–N14–C15–N16 35, O9–N10–C11–N13 14	δCN
714	685	31	N13–C11–N12–H37 55, O9–N10–C11–N13 31	ρNH
696	668	1	N4–C1–N3–H24 24, N21–C19–N18–H47 18, N21–C19–N20–H46 13, N4–C1–N3–H42 11	ρNH
673	646	40	O5–S6 34, S6–O8 33, S6–O7 12, S6–O9 11	δSO
597	573	14	N18–C19–N20 54, N18–C19–N21 24, N2–C1–N3 11	δCN
589	565	54	N10–C11–N12 41, N10–C11–N13 33	δCN
587	564	76	N3–C1–N2–H44 26, N2–C1–N3 22, N3–C1–N4–H43 20	δCN, ρNH
573	550	17	N2–C1–N3 31, N14–C15–N16 14, N14–C15–N17 13	δCN, ρNH
573	550	28	N2–C1–N3 17, N12–C11–N13–H25 13, N14–C15–N17 13, N13–C11–N12–H27 12, N14–C15–N16 11	δCN, ρNH

TABLE IV — cont.

Frequency [cm^{-1}]	Scaled frequency [cm^{-1}]	Intensity [km/mol]	PED % (more than 10%)	A
569	546	357	N12–C11–N13–H25 28, N13–C11–N12–H27 25, N14–C15–N17–H41 10, N14–C15–N16–H40 10	ρNH
565	542	180	N14–C15–N16–H40 31, N14–C15–N17–H41 31, N14–C15–N16 17	ρNH, δCN
558	536	272	N20–C19–N21–H31 32, N21–C19–N20–H32 28, N3–C1–N2–H44 13, N3–C1–N4–H43 11	ρNH
540	519	15	N2–C1–N4 81	γCN
534	513	4	N10–C11–N13 47, N10–C11–N12 28	γCN
528	507	12	N14–C15–N17 39, N14–C15–N16 31	γCN
528	507	6	N18–C19–N21 43, N18–C19–N20 24	γCN
460	441	144	N2–O5–S6–O8 40, O5–S6–O9 22	γSO
449	431	51	N2–O5–S6–O7 38, N2–O5–S6–O9 20, O5–S6–O8 10	γSO
425	408	33	O5–S6–O7 29, O5–S6–O8 28, O5–S6–O9 21	γSO
373	358	5	O5–S6–O9 23, N3–C1–N4–H43 19, N3–C1–N2–H44 14, N2–O5–S6–O8 12	γSO, ρNH
357	343	17	N3–C1–N4–H43 31, N3–C1–N2–H44 23, O5–S6–O9 16	ρNH, γSO
348	334	7	N14–C15–N17–H41 41, N14–C15–N16–H40 38	ρNH
334	321	5	N13–C11–N12–H27 43, N12–C11–N13–H25 36	ρNH
318	306	13	O5–S6–O8 43, O5–S6–O7 22, N2–O5–S6–O9 21, O9–N10 12	γSO
315	302	4	N21–C19–N20–H32 49, N20–C19–N21–H31 37	ρNH
231	222	93	O8–N18 31, N2–O5 26, S6–O9–N14 19, O8–N18–C19–N21 12, C1–N2–O5–S6 10	L
219	210	27	S6–O8–N18–C19 30, C19–N20–CL22 23, C1–N2–O5–S6 18, N20–CL22 15, N2–O5–S6 13, O9–S6–O8–N18 11, O5–S6–O9 10	L
217	208	25	C19–N20–CL22 30, N10–CL23 22, O8–S6–O9–N14 15, C11–N10–CL23 14, N2–O5 10	L
208	199	22	N10–CL23 43, O8–S6–O9–N10 36, S6–O9–N10–C11 19, S6–O9–N14 11	L
193	186	3	C1–N2–O5 60, N21–C19–N20–CL22 19, O5–S6–O9 16	L
192	184	26	S6–O9–N10 27, O9–N10 13, O9–N10–C11–N13 11, O9–N14 10	L
189	181	9	C11–N10–CL23 39, S6–O9–N14–C15 19, N13–C11–N10–CL23 17, O9–N10 14	L
179	172	2	O9–N10–C11 41, O9–N10 21, O8–N18–C19 14, C19–N20–CL22 12, O9–N10–C11–N13 12, S6–O9–N14 12, O8–S6–O9–N14 11, N21–C19–N20–CL22 10	L
172	165	29	O9–N10–C11–N13 21, O8–S6–O9–N14 17, N2–O5–S6 12	L
165	159	10	O8–N18–C19–N21 45, N21–C19–N20–CL22 22, S6–O9–N14 19, N3–C1–N2–O5 10	L
161	154	12	N21–C19–N20–CL22 23, O8–N18–C19–N21 22, N2–O5–S6 17, N20–CL22 14, N13–C11–N10–CL23 12	L
158	152	0	C1–N2–O5 26, O9–N10–C11 13, N2–O5 10	L
153	147	1	O9–N14 31, O9–N10–C11–N13 23, N13–C11–N10–CL23 18	L
139	133	2	O9–N14–C15–N16 30, S6–O9–N14–C15 22, O9–N14–C15–N17 21, O9–N10–C11 17, S6–O9–N10–C11 15	L
138	132	4	S6–O9–N14 30, O9–S6–O8–N18 26, C1–N2–O5–S6 19, N20–CL22 12, N21–C19–N20–CL22 11	L
130	125	2	N3–C1–N2–O5 29, N2–O5–S6–O7 15, O8–N18 12, N20–CL22 10	L
126	121	1	C1–N2–O5–S6 28, N3–C1–N2–O5 26, O8–S6–O9–N14 20, C19–N20–CL22 12	L
121	116	8	O9–N10–C11–N12 32, N13–C11–N10–CL23 28, O9–N10–C11 18	L
114	109	6	O8–N18–C19–N20 60, O8–N18–C19 16, O8–N18–C19–N21 12, N21–C19–N20–CL22 11	L

TABLE IV — cont.

Frequency [cm^{-1}]	Scaled frequency [cm^{-1}]	Intensity [km/mol]	PED % (more than 10%)	*A*
105	101	8	O9–N10–C11–N13 40, N13–C11–N10–CL23 37, C11–N10–CL23 23	L
94	91	6	S6–O8–N18–C19 63, O9–N14–C15 23	L
80	77	2	N2–O5–S6–O8 50, S6–O9–N10 24, S6–O9–N10–C11 13, N2–O5–S6–O7 12	L
78	75	9	O8–N18–C19 27, O8–S6–O9–N14 26, S6–O8–N18 11, C19–N20–CL22 10, S6–O9–N10–C11 10	L
68	65	2	S6–O8–N18 32, O8–S6–O9–N10 27	L
63	60	5	N2–O5–S6 37, O9–N14 23, S6–O9–N10 17, O8–S6–O9–N10 15	L
46	44	10	S6–O9–N10–C11 56, O9–N14–C15 16, S6–O8–N18 11, S6–O9–N14–C15 11	L
37	36	4	N2–O5–S6–O9 48, S6–O8–N18–C19 25, N2–O5–S6 18	L
34	32	2	S6–O8–N18–C19 31, S6–O9–N10–C11 14, N2–O5–S6 14, S6–O8–N18 13, S6–O9–N14 12, O8–S6–O9–N10 12	L
21	21	4	O8–S6–O9–N10 30, N2–O5–S6–O8 22, S6–O9–N10–C11 18, N2–O5–S6–O9 14, O8–S6–O9–N14 12	L
17	17	0	O9–S6–O8–N18 34, N2–O5–S6–O9 24, S6–O9–N10–C11 22, S6–O8–N18–C19 15	L

A — assignment; ν — stretching; s — symmetric; as — antisymmetric, δ — in plane bending symmetric; γ — in plane bending antisymmetric; ω — out of plane bending symmetric; ρ — out of plane bending antisymmetric; L — libration